minerals

MDPI

Article

Geometallurgy of Trace Elements in the Hrazdan Iron Deposit

Rob Bowell [1,*], Christopher Brough [2], Andrew Barnes [3] and Arman Vardanyan [4]

[1] SRK Consulting, Cardiff CF10 2HH, UK
[2] Petrolab Limited, Redruth TR15 3AE, UK; chris@petrolabs.com
[3] Geochemic Ltd., Abergavenny NP4 5UH, UK; abarnes@geochemic.co.uk
[4] Hzradan Mining Company, Yerevan 0010, Armenia; arman.vrd@gmail.com
* Correspondence: rbowell@srk.co.uk; Tel.: +44-47385379991

Abstract: This study presents an evaluation of arsenic and other trace metals in the Hrazdan Iron-Ore project in Armenia using a methodology typically associated with Geometallurgical characterization. The principal host of the trace elements is pyrite and oxidized equivalents. Pyrite is a mineral of elemental concern as it has the potential to generate acidic pH in water that it contacts and thus mobilize metals of concern. In the Hrazdan deposit, there is a general excess of neutralizing carbonate minerals that result in adequate buffering of generated acid and limiting the mobility of metal cations in solution. However, metalloids that form oxyanions species such as those of arsenic or chromium tend to be more mobile in neutral to alkaline mine drainage. From the geometallurgical assessment of the mine waste, the results of the geochemical testwork can be explained and the information used to assess potential issues with mine waste storage, timing of metal release and provide a baseline for mitigation strategies.

Keywords: geochemistry; waste rock; pyrite; arsenic; iron ore

Citation: Bowell, R.; Brough, C.; Barnes, A.; Vardanyan, A. Geometallurgy of Trace Elements in the Hrazdan Iron Deposit. *Minerals* **2021**, *11*, 1085. https://doi.org/10.3390/min11101085

Academic Editor: Anita Parbhakar-Fox

Received: 1 September 2021
Accepted: 28 September 2021
Published: 2 October 2021

1. Introduction

For acid rock drainage and metal leaching (ARDML), one of the principle problematic minerals of interest is the sulfide pyrite. This is primarily due to higher natural abundance in comparison to other sulfide minerals and its acid-generating properties during natural weathering. However, pyrite may also be environmentally problematic even when abundant neutralising minerals are present. This is because it may contain trace elements that are geochemically mobile in circum-neutral pH, such as arsenic.

There has been a growing acceptance and use of the same techniques of geometallurgy (such as mineralogy and diagnostic leaching) to mine wastes to explain observations from geochemical testwork or predict potential environmental issues [1–3]. The weathering and gradual oxidation of sulfides, and in particular pyrite, has the potential to result in acid-rock drainage and metal(loid) leaching (ARDML) [4–6]. This process is accelerated during mining due to the increased likelihood of sulfide exposure, effectively accelerating the natural weathering process. For ARDML the main deleterious minerals are the sulfides, and of these, due to its greater natural abundance the main contributor to ARDML is pyrite [5].

The general Equation (1) for pyrite oxidation is summarized below:

$$4FeS_2(s) + 15O_2(g) + 14H_2O(l) \rightarrow 4Fe(OH)_3(s) + 8SO_4^{2-}(aq) + 16H^+(aq) \quad (1)$$

Along with the abundance of pyrite present in the mine waste and the balance of available neutralizing minerals it is important to consider textural controls [1,2] and pyrite trace element content [7–12] when assessing the ARDML potential, especially as the release of potentially problematic concentrations of metals can still be associated with circum-neutral leaching conditions [13]. Pyrite trace element has been linked to increased weathering rates, whether through the presence of inclusions that destabilise the crystal

lattice [7,14,15] or the presence of arsenic in solid solution [2,15–17]. In the last two decades, in situ trace element analysis has been developed to analyse and quantify the trace element content of pyrite is a potential core component of assessing the metal(loid) (this term is used to group transition metals and semi-metals of groups III, IV and V that show metallic properties) leaching risk of potential mine waste [9–12,15,18] and has been used to assess metal concentrations in mine waste at the Baal Gammon mine [19] and Tools [20], both in Australia. One such approach is Laser Ablation Inductively Coupled Mass Spectrometry (LA-ICP-MS) that allows analysis of trace elements within mineral grains as small as 10 μm or less [10,15].

This paper presents a case study where such an approach was applied to identify the source of elements of concern in mine waste from the Hrazdan Iron ore project in Armenia.

1.1. Location

The Hrazdan project is located 1.5 km from the city of Hrazdan and 50 km north-east of the Armenian capital, Yerevan (Figure 1). The deposit itself is classed as an iron-magnetite skarn hosted within two separate tabular shears. It is anticipated that the project will develop as one main pit with multiple waste rock facilities that will be located adjacent to major surface water system (Figure 1). As such it is critical to ensure a comprehensive understanding of the material properties and likelihood to generate leachate that could impact the water courses.

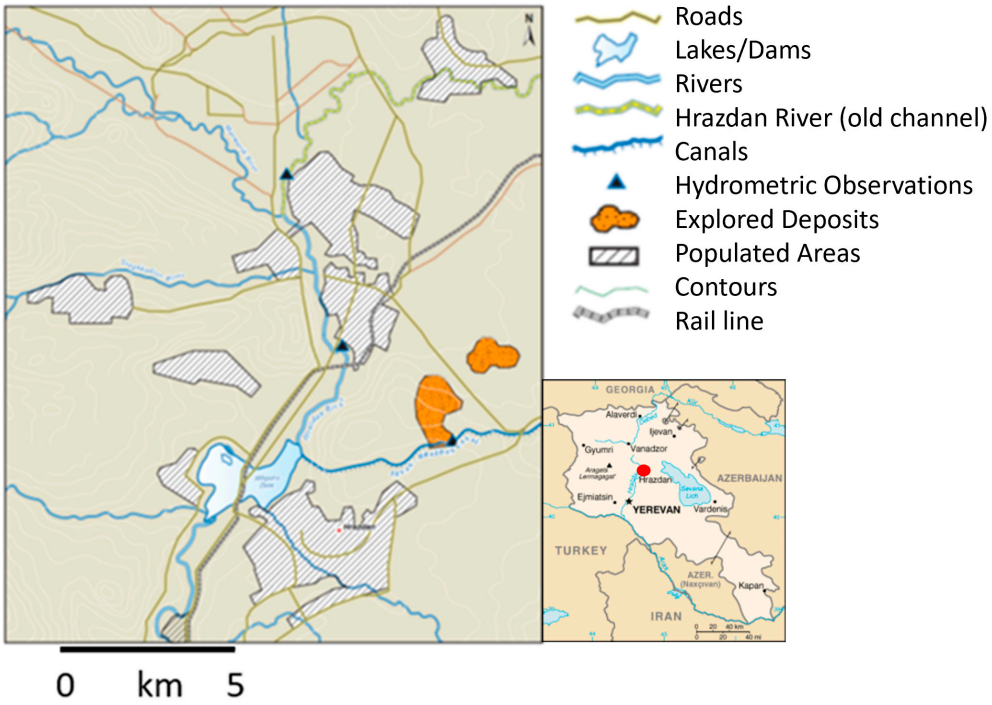

Figure 1. Location map (insert map shows location of Armenia and Hzradan to the north of Yerevan, the capital as a red dot).

1.2. Geological Setting

Armenia lies principally within the Lesser Caucasus terrain of the Caucasus region. Sub-terrain accretion occurred along a WNW–ESE trend, reflected in the direction of a number of the major faults traced across the country. The Somheto-Karabakh sub-zone of the Lesser Caucasus consists mainly of Jurassic and Cretaceous age rocks that host skarn deposits, porphyry coppers and vein-type deposits associated with Late Cretaceous to Paleogene intrusion [21]. One of the main outcrops of Precambrian metamorphic

basement rocks in Armenia is located in the basin of Hrazdan. Predominately, however, the area is covered by Quaternary lithologies, including Pliocene lavas aged 5–10 Ma [22]. The area lies in the Arpa-Vorotan zone of uplifts and troughs, which correspond to a major Paleogene syncline. This contributed to the total uplift of 1.8 km in the whole of the Lesser Caucasus terrain [23,24].

The deposit is mainly hosted by the Lower Paleozoic (Eopalaeozoic) Hankavan schist complex along with the overlying Cretaceous-Tertiary carbonate sandstones. The Paleozoic schist represents metamorphosed shales, with chlorite, chlorite-epidote, epidote-hornblende and micaceous-quartz varieties. Upper-Cretaceous (Senonian) formations are lain unconformably on the lower Paleozoic sediments. These formations are represented by calcareous sandstones, which as a result of contact influence of subsequent acidic intrusions are almost entirely metamorphosed into skarns and hornfels comprising garnet, epidote, pyroxene and, less frequently, actinolite and other accessory minerals [25]. Contact-metamorphic (hornfels-formation) and metasomatic (skarnification) processes have affected all of the host lithologies of the Paleozoic, Senonian and the minor lithologies of the Lower and Middle Eocene ages. These processes were caused by the emplacement of intermediate to acidic intrusions during the Eocene–Miocene ages. Additionally, found within the area are lower Paleozoic metamorphosed porphyries, tuffites and slates, along with Late Oligocene to Early Miocene porphyroid granitoids and the Atisskaya Suite which dates to Middle Plicocene and consists predominantly of pumice sand and liparites [26]. The geological map of the area are shown in Figure 2.

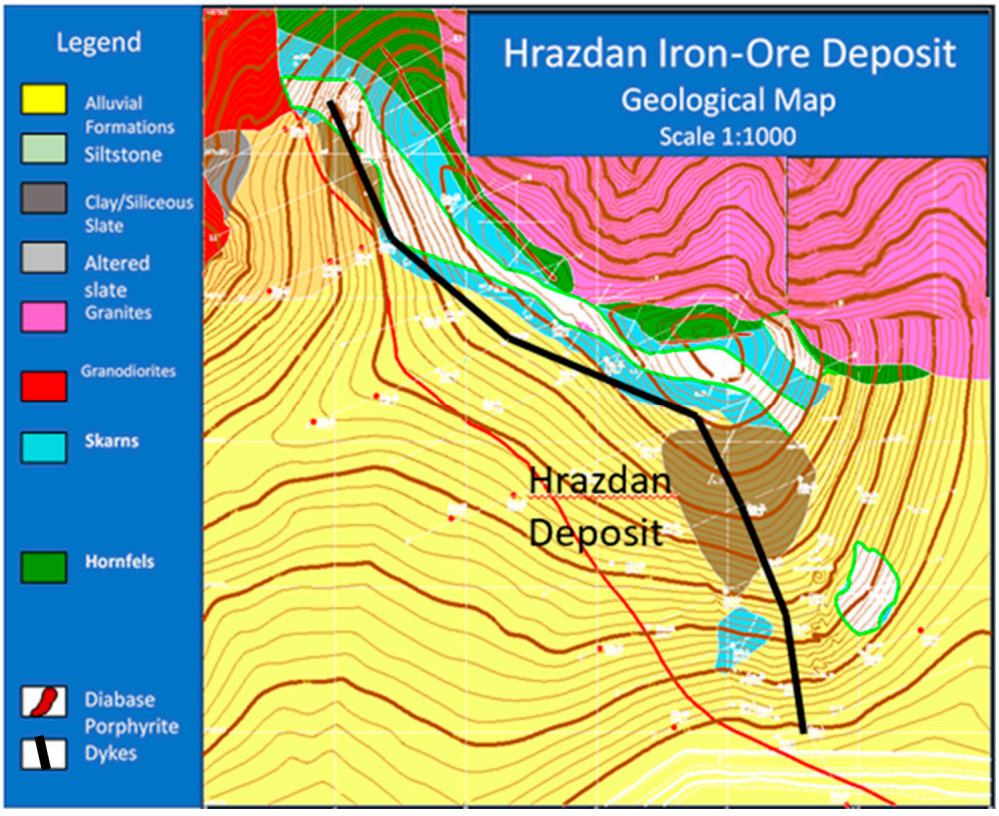

Figure 2. Geological map, Hzradan deposit [27].

The Hrazdan deposit is classed as an iron magnetite skarn. The term 'skarn' refers to the metasomatic replacement of carbonate rocks by calc-silicate assemblages such as Ca-rich garnet, pyroxene, amphibole and epidote. This occurs due to contact or regional metamorphism. The Hrazdan ore deposit is a typical iron-magnetite skarn formed through the metasomatic replacement of calcite-bearing rocks. The deposit is hosted within garnet-

epidote dominated skarns and hornfels, which form the contact lithologies to granite intrusions emplaced in the Lower Eocene to the north.

1.3. Mineralization

Magnetite mineralization is associated with garnet and epidote which simultaneously formed along with massive ores and minor breccias and vein infill. The magnetite mineralization occurs within a series of tabular or lens like bodies with flat and inclined bedding extending along strike for 1100 m at a dip of 15° to 30°. The extent of the ore body is reportedly limited to the south-west by a strike-slip fault [28].

Ore mineralogy is subdivided into massive ore or ore skarns. There are several ore types, with different lithologies hosting mineralization, all are characterized by different textures. The ores with massive texture are usually characterized by small to medium grained minerals, consisting mainly of euhedral grains of magnetite and a small amount of non-metallic minerals. The banded massive texture displays alteration of medium grained magnetite with thin bands of disseminated ores and barren skarns. The disseminated ore marks the gradational boundary between massive ore and barren skarns. Uniformly disseminated textures are characterized by even distribution of magnetite grains within a mass of non-metallic minerals. Banded disseminated texture is identified by alternating bands of magnetite enriched rock and barren skarn. The thickness of the band's ranges from 1 to 10 mm. Non-uniformly and mottled disseminated textures are characterized by uneven distribution of magnetite among non-metallic minerals. The breccia texture is a local development and in most cases is related to post-ore deformation. Fragments of massive and disseminated ores are cemented by chlorite, epidote, and other minerals, or occasionally by granodiorites. Ores with vein textures are usually skarns with anastomosing veins of magnetite. Massive and banded ore textures are the most common, however, it can be difficult to distinguish between these textures as many of the boundaries are gradational. In thin section the ore is reportedly identical in composition.

The massive ores often form pinching and branching tabular aggregations, size ranging from tens of centimeters to up to several meters. In rare cases there are sharp contacts of massive ore with barren metasomatic rocks and diorite intrusions, more often they are associated with a gradual transition into disseminated ore, often classed by its predominant mineralogy. The garnet-magnetite ores are the most disseminated and can occur as thin discreet units alternating with massive ores, or at the contact between ore and barren skarn, or in rare cases as a unit within barren rock. Characteristically the unit is identified by a sharp increase in the predominance of garnet and magnetite. The garnet-epidote-magnetite ores have a limited distribution. The magnetite in these is non-uniformly disseminated, sometimes veining. The magnetite forms isometric phenocrysts. The epidote-scapolite-magnetite ores are rare, mainly found in the north-western part of the deposit occurring as tabular bodies.

Based on the geological information and previous observations made during drilling and aquifer testing in the area, it is inferred that most of the rock mass within the project area can be described as minor or non-aquifer media. The top weathered and fractured horizons form a thin cover aquifer. Therefore, it is expected that drainage of the rock mass is primarily fracture driven flow. Any significant groundwater flow is limited to the fractured horizons.

The groundwater flow pattern broadly mimic, the topographic contours, suggesting that the aquifers are recharged by precipitation and drain under gravity toward the Hrazdan River. This will therefore be the main direction of travel for any leachate from the waste rock facilities for which the geochemical assessment has been undertaken (Figure 3).

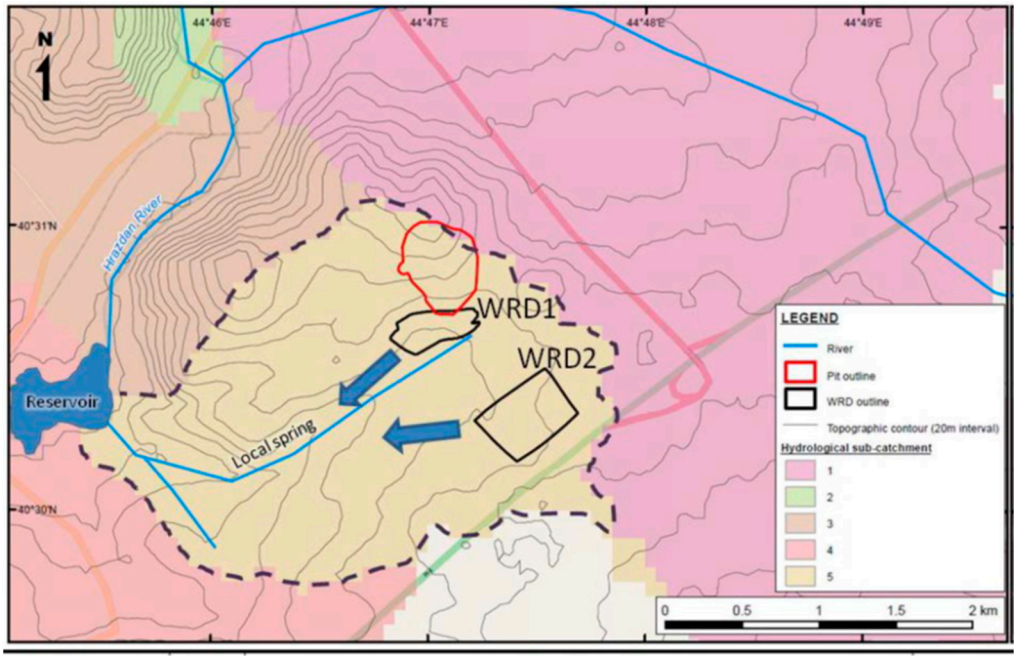

Figure 3. Simplified illustration of the mine plan for Hrazdan showing the pit outline and the two-waste rock (WRD) dump outlines. The waste facilities are situated within the same hydrological sub-catchment which would drain towards the reservoir. Dashed line shows mining area.

2. Materials and Methods

2.1. Samples

Fifty samples were collected for initial assessment of waste rock mineralogy and geochemistry [28]. These were used for the initial mineralogy, acid generation and metal content testwork. From this data set six samples representative of mine waste from the Hrazdan Iron-Ore project were selected for humidity cell testing, diagnostic leach tests and high precision Laser ICP-MS examination (Table 1). These included the four of the most problematic (in terms of sulfide content and metal(loid) release during static testing) waste-rock lithologies from the static tests, along with two composites representative of the bulk mineralogy of the overall waste rock. Composites were prepared by taking 250 g of unpulverized material from each of the original waste rock samples of appropriate mineralogy. The bulk was then riffle split down for the subsequently required testwork. Whole rock geochemistry of the samples indicates a Geochemical Abundance Index > 3 indicates greater than 12 times average crustal abundance [29].

Table 1. Summary of ARDML indicators for the main waste rock types.

Rock Type	NNP[1], Mean	NPR[2], Mean	GAI[3]-As, Mean
Skarn Ore	−0.6	1.9	12
Skarn waste	7.9	22	21
Slate	21	48.4	3.4
Siltstone	22.3	50	1.9
Chert (altered slate)	−0.4	1.6	12

Note: [1]NNP = Net Neutralization Potential, [2]NPR = Neutralization Potential Ratio, [3]GAI = Geochemical Abundance Index.

2.2. Mineralogy

A mineralogical examination was undertaken on a selected subset of ten samples of core material. This was done using petrographic microscopy (both transmitted and reflected light), scanning electron microscopy (SEM) with quantitative elemental analysis using Energy Dispersive X-Ray (EDX) and fine powder X-Ray Diffraction (XRD) analysis at Cardiff University, Cardiff, UK. Samples were prepared from core as polished thin section (for optical microscopy and SEM) and XRD analysis was carried out on the less than 100 μm fraction of the pulverized sample.

2.2.1. Optical Microscopy

The principal method of mineralogical analysis used for this study is Optical Microscopy. This was completed on polished thin sections of core material. A Meiji MX9000 microscope fitted with a mounted Canon EOS 300D digital camera has been used in this study.

2.2.2. Scanning Electron Microscopy

A Scanning Electron Microscope with Oxford Instrument "INCA" system wave- and energy-dispersive X-Ray spectroscopy was utilized for semi-quantitative analysis of minerals present within the polished thin sections. This method allows micro-chemical data to be collected that reports the chemical composition of the surface of the mineral phase in the polished section. The electron beam utilized to gather the information required is approximately 1 to 5 μm in diameter, so even very small phases can be quantified.

2.2.3. X-ray Diffraction

X-ray Diffraction analysis was carried out using a Philips PW1710 Powder Diffractometer at the Department of Earth Science, Cardiff University, UK. Bulk analyses were carried out on samples. Scans were run using Cu Kα radiation at 35 kV and 40 mA, between 2 and 70° 2θ at a scan speed of 0.04° 2θ/s. From the scans, phases were identified and from the peak areas, semi quantitative analysis was performed, and a percentage of each phase present calculated.

2.3. Assessment of Acid Generation

Acid Base Accounting (ABA) indicates the theoretical potential for a given material to produce net acid conditions. The approach does not take into account mineralogy, kinetics or other influencing factors controlling natural sulfide oxidation. The technique can be considered as characterizing the 'total potential reservoir of acidity or alkalinity in a given material.

The ABA testwork was used to determine the acid generating potential (AP) and neutralising potential (NP) of each sample based on sulfide sulfur and inorganic carbon content, respectively. ABA entails complete combustion of a sample in a Leco furnace and determination of the CO_2 and SO_2 given off from the sample. This allows calculation of the total sulfur and carbon content of the material. A duplicate sample is then pre-washed with a weak hydrochloric acid to remove the inorganic carbon and sulfates, thereby allowing the speciation of carbon and sulfate in the material to be determined. Results are expressed as kg $CaCO_3$ equivalents per ton. From the values of AP and NP it was then possible to determine the net neutralization potential (NNP) and neutralization potential ratio (NPR) of each sample as follows:

$$\text{Net Neutralizing Potential (NNP) (kg } CaCO_3 \text{ equivalents per ton)} = NP - AP$$

$$\text{Neutralization Potential Ratio (NPR)} = NP/AP$$

The balance between the acid generating mineral phases and acid neutralising mineral phases is referred to as the net neutralization potential (NNP), which is equal to the

difference between NP and AP. The NNP allows classification of the samples as potentially acid consuming or acid producing. A positive value of NNP indicates the sample neutralizes more acid than is produced during oxidation. A negative NNP value indicates there are more acid producing constituents than acid neutralising constituents.

The results of ABA testwork are invaluable in determining the potential for acid generation from each lithology and data were interpreted using the criteria outlined in Table 2. For samples where the NNP and NPR do not lie within the same field (e.g., NPR < 1 but NNP > −20) the worst of the two cases is taken (i.e., in the example the material would be classed as potentially acid forming).

Table 2. Interpretation of ABA data [29].

Catergory	NNP[1] (eq kg $CaCO_3$/t)	NPR[2]
Potentially Acid Forming, PAF	x < −20	x < 1
Uncertain Prediction	−20 < x < +20	1 < x < 3
Non Acid Forming, NAF	x > +20	x > 3

Note: [1]NNP = Net Neutralization Potential, [2]NPR = Neutralization Potential Ratio.

A multi element analysis of the waste materials was completed to provide an absolute upper limit of available metals for leaching from the samples. The analysis involved a strong multi acid digestion using a combination of concentrated hydrofluoric (HF), nitric (HNO_3), hydrochloric (HCl) and perchloric ($HClO_4$) acids. This is followed by analysis by ICP-OES and ICP-MS for a full suite of metals and metalloids, including determination of major elements (e.g., aluminium, calcium, magnesium, sodium, potassium, iron, sulfur) and trace elements (e.g., zinc, copper, cadmium and lead). The results of the multi element analysis were analysed using the Geochemical Abundance Index (GAI) [29] which compares the concentration of an element in each sample to its average crustal abundance. GAI values are particularly useful in determining the relative enrichment of elements based on lithology and may be used to identify elements enriched above average crustal concentrations. GAI values are calculated as follows:

$$GAI = \log[C/(1.5*S)]$$

where C is the concentration of an element as determined from the multi element assay and S is the average crustal abundance of the element of interest [30]. Materials are then assigned a GAI value between zero and six based on the degree of enrichment (Table 3). According to the GARD protocol [29], a GAI value greater than three indicates significant enrichment.

Table 3. Categories applied to GAI values [29].

GAI Value	Interpretation
0	<3 times average crustal concentrations
1	3 to 6 times average crustal concentrations
2	6 to 12 times average crustal concentrations
3	12 to 24 times average crustal concentrations
4	24 to 48 times average crustal concentrations
5	48 to 96 times average crustal concentrations
6	>96 times average crustal concentrations

2.4. Leach Tests

Two static leach tests were developed. The first utilized deionized water leach carried out to give an indication of short-term metal mobility and to identify constituents that are immediately available for release. For this project a single stage extraction was performed using liquid: solid ratio of 10:1 and agitation for 24 h on crushed material <6 mm. The eluate was then filtered, and measurements were made for pH, conductivity and for a

suite of cations and anions. The leach was carried out in accordance with the Australian Standard AS 4439.3 [31] to determine the components that are immediately available for release from the samples.

In addition, a hydrogen peroxide leach was also undertaken with analysis for dissolved metals/metalloids by inductively coupled plasma-optical emission spectrometry/inductively coupled plasma-mass spectrometry (ICP-OES)/(ICP-MS) following filtration to <0.45 μm. As the aggressive oxidising conditions of the hydrogen peroxide should leach all physically exposed or chemically available sulfide minerals, this gives an indication of the potential for high level metal release that would occur during exposure of the material to oxygen.

2.5. Kinetic Testing

The kinetic tests were carried out according to the ASTM D 5744-13e1 standard methodology [31,32] HCT and were run for a total of 144 weeks. Under ASTM methodology, the test followed a seven-day cycle. This consists of 3 days circulating dry air, 3 days circulating humid air (at 25 °C) followed by a leach day in which the column is flooded with deionized water prior to draining and leachate collection. Following overnight draining, the cycle is restarted. Each week the collected leachate was filtered through 0.45 μm membrane filters prior to analysis for major cations and anions, trace elements, pH and electrical conductivity. The pH meter was a Metrohm Titrando (Metrohm, Switzerland) with I electrode plus. It was calibrated daily with NIST standards at pH 1.68, 4.0, 7.0 and 10.0. pH 4.0 and 7.0 standards were checked every 10 samples and the meter was recalibrated as necessary. The EC meter was an Oakton Con 700 (Oakton, Chicago, IL, USA). It was calibrated daily with commercial standard (Thermo Orion, Thermo Fisher Scientific, Waltham, MA, USA) at an EC of 1413 μS/cm. The standard was checked every 10 samples with the meter recalibrated as necessary. The ICP analysis was calibrated before each run and subsequently every 10 samples using a blank and a standard. After 20 weeks the results were evaluated to assess the initial results.

2.6. Selective Extraction Testwork

A summary of the extraction methodology used in this test work programme is presented in Figure 4. The individual extraction procedures are described in more details below.

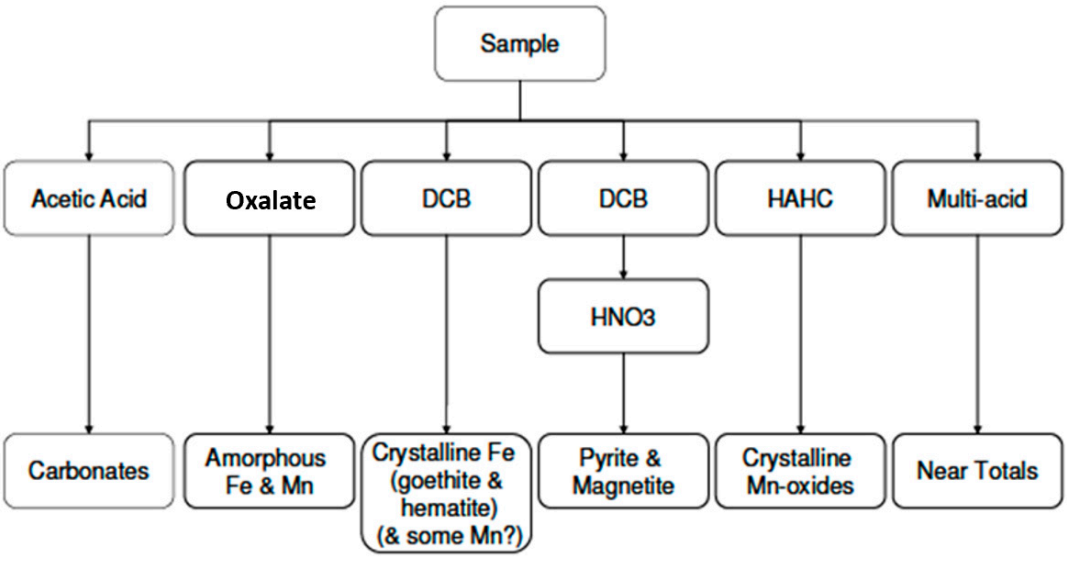

Figure 4. Selective Extraction Scheme.

2.7. Amorphous Iron Oxides (Oxalate Extraction (OX))

The oxalate extraction procedure of Schwertmann and Cornell [33] was employed using 40 mg samples in 40 mL of 0.2 M oxalic acid-0.2 M ammonium oxalate adjusted to pH 3. All extractions were conducted in the absence of light under constant agitation for 4 h using an end-over-end rotator. Upon completion of the extraction phase, supernatants were recovered by centrifugation and immediately filtered through 0.45 μm MCA membranes prior to analysis.

2.8. Crystalline Iron Oxides (Dithionite Citrate Bicarbonate Extraction (DCB))

Dithionite Citrate Bicarbonate (DCB) extractions were undertaken to determine elements associated with crystalline iron oxides [34]. 400 mg samples were extracted in 400 mL of citrate bicarbonate buffer at pH 7.3 and brought to 80 °C under constant stirring. 10 g of sodium dithionite was introduced into extraction vessels and maintained at 80 °C whilst the reaction was allowed to proceed to completion (circa. 40 min). Supernatant samples were recovered by centrifugation and immediately filtered through 0.45 μm MCA membranes prior to analysis.

2.9. Sulfides and Magnetite by Sequential Extraction (DCB + Nitric Extraction (DCBN))

Sulfides (and residual magnetite) were sequentially extracted from the residual pulps recovered from DCB extractions using ASTM 1915. Briefly this method involves boiling the sample in 20% nitric acid for 10 min. The residual pulp is then recovered by centrifugation and dried at 105 °C prior to sulfur determination by high temperature combustion with IR detection. The recovered supernatant is analysed for multi-elements following filtration.

2.10. Carbonate (Acetic Acid (AA) Extraction)

An acetic acid/Na-acetate buffered extraction at circa. pH 5 was used to assess geochemical associations with carbonate phases. 2.65 g samples were extracted in 40 mls of acetic acid buffered to pH 5 with sodium acetate. Extractions were carried out for 24 h with intermittent shaking. Upon the termination of the extraction phase, supernatant samples were recovered by centrifugation and immediately filtered through 0.45 μm MCA membranes prior to analysis. Total Inorganic Carbon was analysed on residuals by high temperature combustion with IR detection (Nicolet Nexus 870 FTIR spectrometer with a smart endurance single bounce diamond ATR cell, Bruker, Billerica, MA, USA) and revealed complete dissolution of carbonates (<0.2 wt. % CO_3-C was recorded for all samples).

2.11. Manganese Oxides (Hydroxylamine Hydrochloride Extraction (HAHC))

The cold hydroxylamine hydrochloride extraction procedure was used to selectively dissolve manganese oxides using 0.1 M hydroxylamine hydrochloride in 0.01 M nitric acid. Extractions were conducted at room temperature for 30 min on 40 mg samples in 40 mL extractant.

2.12. Multi-Acid Near Total Digestion (Multi-Acid Digestion (MAD))

Multi-acid near total dissolutions ($HF/HClO_4/HNO_3/HCl$) were undertaken in a Microwave Accelerated Reaction (MARS) using the thermal reaction profile described in USEPA 3052. Dissolutions were made to final dilution and filtered prior to analysis.

All extractions were analysed for the following multi-element suite by ICP-MS; Ag, Al, As, Ba, Be, Bi, Ca, Cd, Co, Cr, Cu, Fe, K, Li, Mg, Mn, Mo, Na, Ni, Pb, S, Sb, Se, Sn, Si, Sr, Ti, Tl, V, Zn and F by spectrophotometric methods.

2.13. Laser ICP-MS

The laser ablation ICP-MS housed at Cardiff University comprises a New Wave UP213 laser system coupled to a Thermo X-Series2 ICP-MS. Matrix matched standards, were used for analyzing sulfides and oxides. Ablation traces were carried out at 15 Hz using helium in the sealed laser cell, and the resulting vapour was combined with argon before delivery into the ICP-MS. Ablations were acquired in time-resolved analysis (TRA) mode and consisted of a spot size approximately 25 μm wide by 20 μm deep and of variable length. Typical acquisitions lasted 80–150 s.

The laser ICP-MS was tuned at the start of the day using NIST 612 to reduce low mass sensitivity while maintaining or enhancing mid to high mass sensitivity. Analytical runs consisted of a calibration block involving measurements of relevant standards followed by NIST612 standards. After background correction of the data, the signals were normalized against the standards and the arsenic content quantified.

3. Results

3.1. Mineralogy

The main minerals observed at Hrazdan are magnetite, garnet, epidote, sericite, quartz, calcite, hematite and iron hydroxides (Figure 5). The magnetite is partially martitized (that is replaced by hematite due to oxidation) occasionally this replacement produces pseudomorphs of hematite. In addition to this there is occasional alteration to limonite which covers the magnetite and hematite producing a flakey texture. The overall presence of iron hydroxides is recorded as minor being present along cracks or the outer edge of quartz-magnetite veins.

Garnet is a constant presence within the ore forming euhedral grains and closely associated with the magnetite. They are occasionally replaced by epidote, magnetite and quartz. Epidote is a constant component of the ores, though generally cracked and poorly formed. It is occasionally found associated with pyroxene, garnet, quartz and feldspar. Calcite is a minor component of the ore. Pyrite, chalcopyrite and chlorite were also observed, though only in the form of single inclusions.

The results of the mineralogical investigation indicate that sulfide-bearing lithologies predominantly contain pyrite (FeS_2) with accessory pyrrhotite ($Fe_{1-x}S$), chalcopyrite ($CuFeS_2$) and pentlandite ($(Fe,Ni)_9S_8$). Other sulfides observed include galena (PbS), millerite (NiS) and gersdorffite (NiAsS) (Table 4; Figure 6). These will provide some acid-generating capacity as well as the potential to release metals such as arsenic, copper, nickel and lead to the wider environment. Sulfides form a minor (1–10%) component of the chert samples (SRK 2425 & SRK 2438) and trace (<1%) component within all other lithologies.

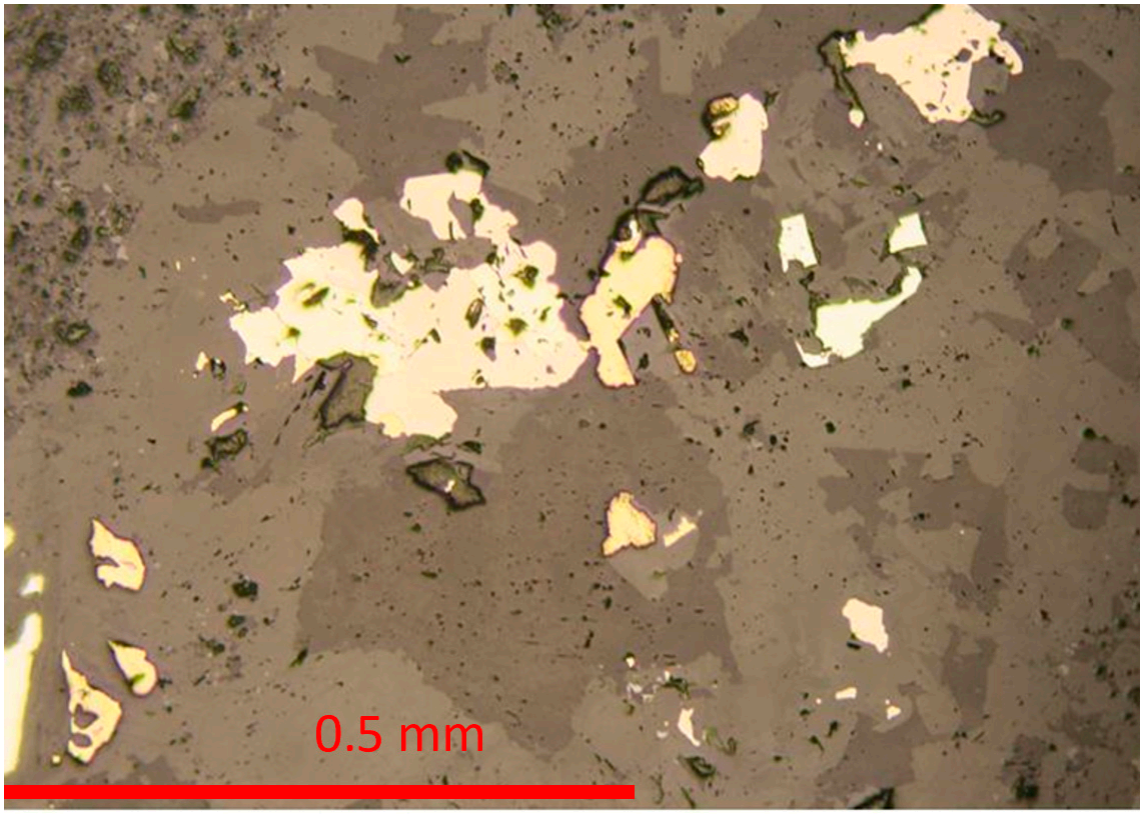

(**A**)

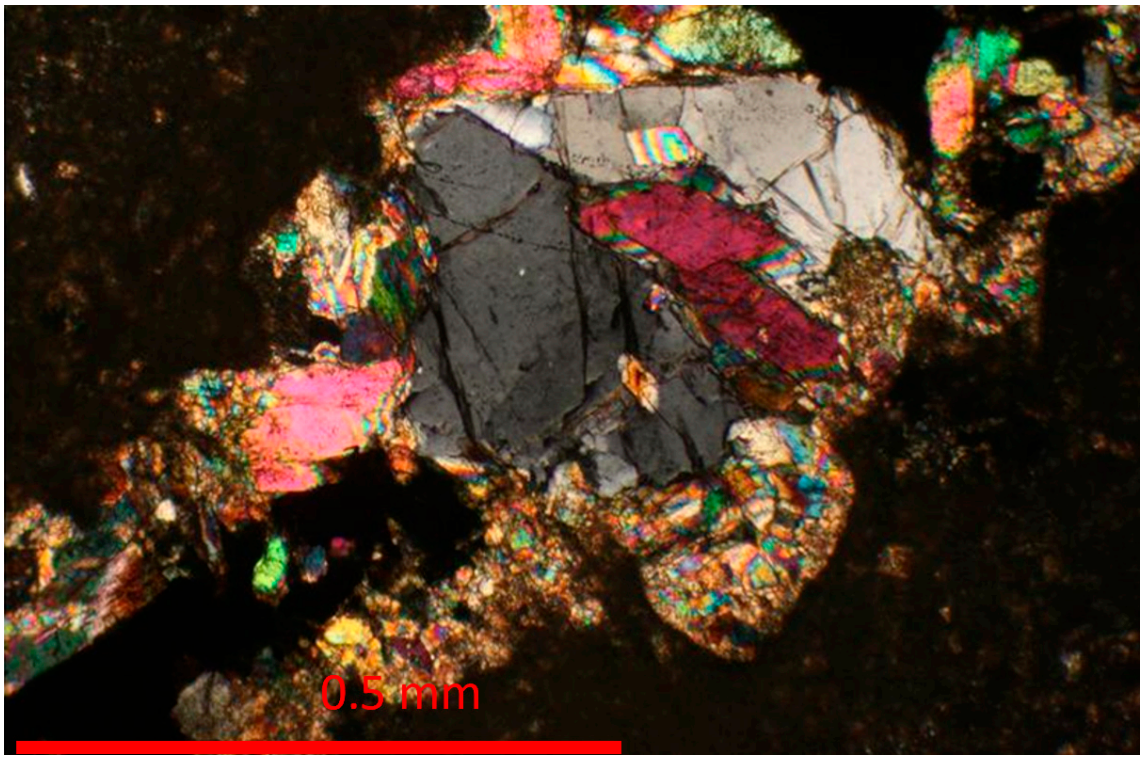

B)

(**C**)

Figure 5. (**A**) Example of sulfides, Hzradan. Pyrite and Chalcopyrite with Arsenopyrite and Tenantite disseminated in the silicate gangue. Field of view is 1 mm. Reflected light; (**B**) Calcite-quartz-epidote skarn showing coarse aggregates of re-crystallized quartz-calcite and epidote porphyroblasts after garnet group phase. Field of view 1 mm. Cross nicol, transmitted light. (**C**) An example of calcite veins cutting through very fine-grained epidote. Field of view 1 mm. Cross nicol, transmitted light.

Acid-neutralizing minerals are present to some extent within all of the samples. In particular calcite is present as a major component within five lithologies and as a minor component within others as vein material (Figure 6). Other acid-neutralising minerals are present in the form of ultramafic and mafic aluminosilicate minerals such as diopside and actinolite. From the visual identification, the proportion of acid-neutralising calcite within the host rock appears to exceed the proportion of acid generating sulfides.

Table 4. Summary mineralogy of selected samples, Hzradan.

Minerals	Sample ID	SRK2424	SRK2425	SRK2430	SRK2438	SRK2558	SRK2563	SRK2570	SRK2572	SRK2574	SRK2579
	Logged Lithology →	**Chert**	**Chert**	**Chlorite-Epidote Skarn**	**Chert**	**Chlorite Skarn**	**Chlorite-Epidote Skarn**	**Chert**	**Chlorite Epidote Skarn**	**Garnet Skarn**	**Chlorite-Epidote Skarn**
	Revised Lithology →	**Diopside Skarn**	**Diopside Skarn**	**Diopside-Epidote Skarn**	**Chlorite-Diopside Skarn**	**Silicified Actinolite-Skarn**	**Garnet Skarn**	**Chert**	**Epidote Skarn**	**Diopside-Epidote Skarn**	**Garnet Skarn**
	Ideal Chemistry ↓										
Quartz	SiO_2			XXX		XXX	XXX	XXX		XXX	XXX
Garnet (Andradite)	$Ca_3Fe^{3+}_2(SiO_4)_3$			XXX			XXX				XXX
Zircon	$ZrSiO_4$	X								X	X
Saponite	$Ca_{0.25}(Mg,Fe)_3((Si,Al)_4O_{10})(OH)_2{\cdot}nH_2O$			XXX						XXX	
Titanite	$CaTi(SiO_4)O$	X	X	X	X	X				X	
Actinolite	$Ca_2(Mg,Fe)_5(Si_8O_{22})(OH)_2$	XX	XX	XX		XXX		X			
Diopside	$CaMgSi_2O_6$	XXX	XXX	XXX	XXX			XXX	XXX	XXX	
Epidote	$Ca_2(Al_2Fe^{3+})(Si_2O_7)(SiO_4)O(OH)$	XX	X	XXX	XX				XXX	XXX	XXX
Oxide Minerals	Ilmenite	$FeTiO_3$					X					
	Haematite	Fe_2O_3						X		X	X	X
	Goethite	FeOOH						X		X	X	
	Magnetite	Fe_3O_4						X			X	X
Phosphates and Sulphates	Fluorapatite	$Ca_5(PO_4)_3F$		X		X	X	X	X			X
	Jarosite	$KFe^{3+}_3(SO_4)_2(OH)_6$						X				
Feldspar Grains	Albite	$NaAlSi_3O_8$				X						
	Labradorite								X			
	Andesine	$(Ca,Na)[Al(Al,Si)Si_2O_8]$	XXX	XXX			XXX		XXX			
	Oligoclase			XX		XXX	X		X			
	Anorthite	$CaAl_2Si_2O_8$		X								
	Anorthoclase	$(Na,K)AlSi_3O_8$		XX					X			
	Microcline	$KAlSi_3O_8$	X				X		X			
Clay Minerals	Kaolinite	$Al_2Si_2O_5(OH)_4$		XX								
	Montmorillonite	$(Na,Ca)_{0.33}(Al,Mg)_2(Si_4O_{10})(OH)_2{\cdot}nH_2O$										XX
	Chamosite	$(Fe^{2+},Mg)_5Al(AlSi_3O_{10})(OH)_8$				X						
	Clinochlore	$(Mg,Fe^{2+})_5Al(AlSi_3O_{10})(OH)_8$	X			XXX			X		X	
Sulfides	Chalcopyrite	$CuFeS_2$		X	X				X			
	Galena	PbS		X								
	Selenian Galena	Pb(S,Se)							X			
	Pentlandite	$(Fe,Ni)_9S_8$		X		X						
	Pyrite	FeS_2	X	XX	X	XX	X					
	Gersdorffite	NiAsS				X						

	Pd-Melonite—Merenskyite	(Pd)$NiTe_2$		X		X						
	Pyrrhotite	$Fe_{1-x}S$		X		X	X		X		X	
	Tsumoite	BiTe				X						
	Millerite	NiS				X						
Carbonates	Calcite	$CaCO_3$	X		XXX	XX	X	XXX		XXX	XXX	XXX

Note: X—Trace Minerals (<1% by area), XX—Minor Minerals (1–10% by area), XXX—Major Minerals (>10% by area).

3.2. Mineral Chemistry

Laser ICP-MS mineralogical analysis was undertaken on several samples to ascertain the primary source of the arsenic in the waste rock. Arsenic was located in several textural locations including (1) one instance of solid solution within calcite, (2) one occasion of an association with fluorapatite (3) several instances of very low concentrations of arsenic associated with iron-oxide material and (4) high concentrations in the trace amounts of pyrite (Figure 6). Of particular interest is the analysis of several pyrite grains from several samples revealed a consistent enrichment of arsenic as solid solution within the rims of the pyrite grains. Percentage concentrations were semi-quantitative but point to values of around 3–4% arsenic within the pyrite rims dropping to ~0.5–1% arsenic within the pyrite cores.

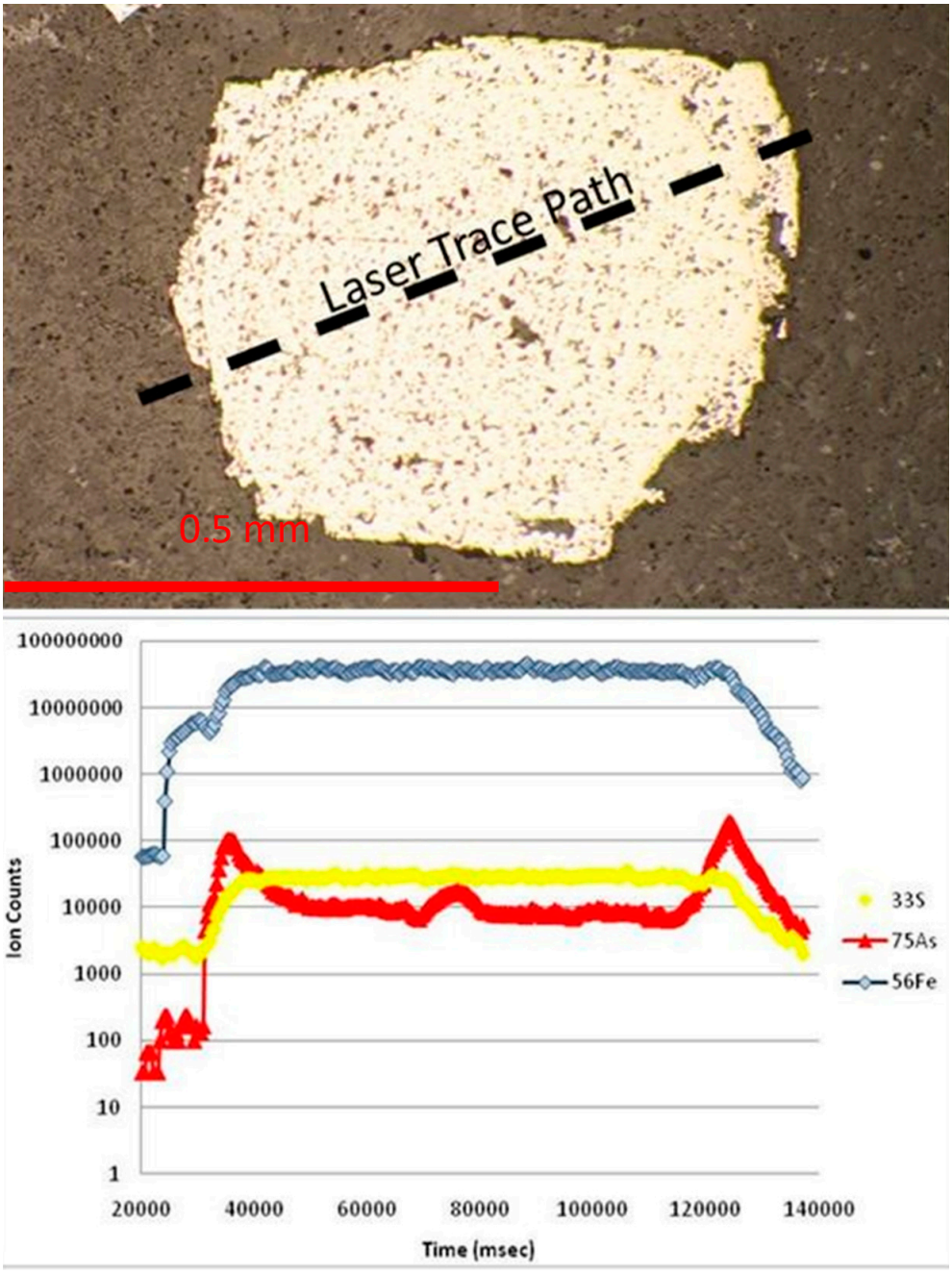

Figure 6. Image showing a pyrite grain and a proposed laser trace. After the trace is performed the graph below shows how the concentrations of key elements vary with time. As can be seen as sulfur and iron values rise (i.e., as you enter the pyrite grain) there is a sharp rise in arsenic values.

3.3. Selective Extraction

From near-total dissolution datasets, samples 1 & 2 have been determined to contain 14 and 46 mg/kg As respectively. As can be observed from, both DCB + OX (crystalline + amorphous iron oxides) and HAHC provide similar recoveries for As suggesting that As may be associated with iron oxide phases (circa. 60–85%), particularly with the predominantly amorphous iron oxides (Table 5). From inspection of data from DCBN extractions, roughly 20% of As appears to be directly associated with the reduced iron sulfide phase pyrite.

From near-total dissolution datasets, samples 3 & 4 have been determined to contain 21 and 20 mg/kg As respectively. Arsenic and Fe in samples 3 and 4 (Table 5) have different geochemical associations than were observed for samples 1 and 2 (SRK2438 and SRK2440). This indicates more reduced conditions associated with these samples with more Fe concentrated in silicate minerals and less iron oxides. Consequently, As is largely associated with pyrite in both samples, although a portion of As in both samples is associated with residual material, presumably as sulfide inclusions in silicates.

This is reflected by the considerably lower leaching potential of these samples observed during humidity cell investigations. This was also reflected in the two composite samples. This reflects the greater presence of iron oxides in these samples.

Table 5. Summary results, Selective Extraction Testwork.

Sample	Element	Amorphous Fe Oxides	Crystalline Fe Oxides	Carbonates	Crystalline Mn Oxides	Pyrite	Sequential Extraction
1	As	10	59.3	14.3	1.7	20	105.3
	Fe	4.89	1.16	0.92	1.24	20.2	28.41
2	As	15.2	45.7	7.17	0.7	18.7	87.47
	Fe	4.3	16.3	1.63	0.7	2.95	25.88
3	As	7.62	9.52	9.52	1.4	50.9	78.96
	Fe	2.72	0.55	1.18	3.36	1.75	9.56
4	As	0	10	11	7	70	98
	Fe	16.1	3.56	3.15	0.44	44.4	67.65

3.4. Acid Base Accounting

As part of the geochemical risk assessment, it was demonstrated (by Acid-base accounting and Net-Acid Generation testwork) that the significant majority of waste rock at Hrazdan can be classified as non-acid forming material [28]. The waste rock consisted primarily of diopside skarn, diopside-epidote skarn and garnet skarn lithologies with generally low sulfide content and moderate to high carbonate content (Figure 7).

The sulfide sulfur content of the core samples varied from below analytical detection limits to a maximum of 0.69 wt% in one sample of fresh high sulfur chert. In general, the samples were characterized by low sulfide contents (less than 0.05 wt%), which is indicative of non-acid forming characteristics.

The following material types can be classed as non-acid forming: chlorite-epidote skarn, low-sulfur chert and garnet skarn. In contrast, the chlorite skarn and the chert high-sulfur materials can be classed as uncertain to potentially acid forming based on the results of acid base accounting testwork (Figure 8).

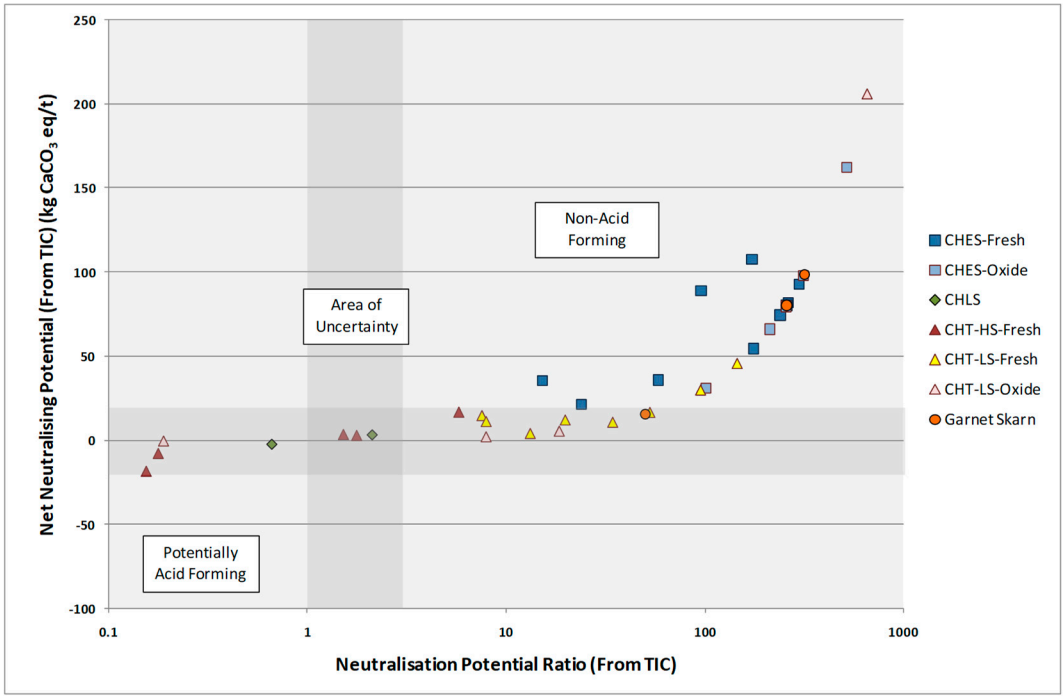

Figure 7. Scatter plot comparing NPR and NNP of the core samples. Both calculated from total inorganic carbon.

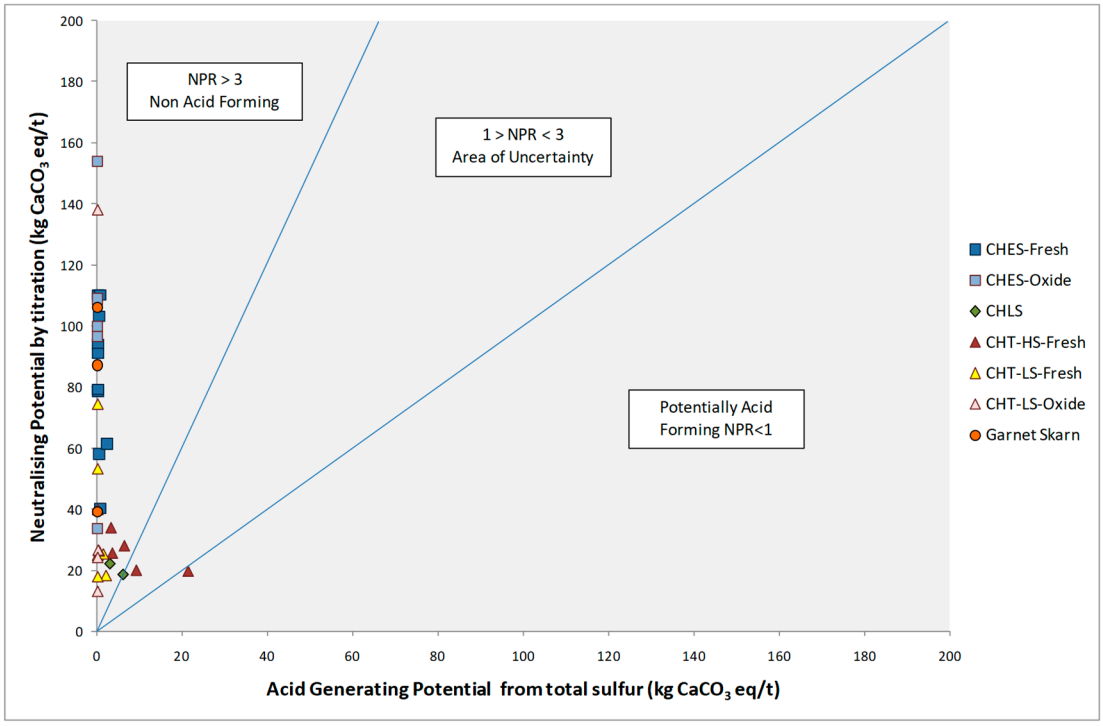

Figure 8. Scatter plot comparing acid generating potential and neutralising potential of the waste rock material.

3.5. Total Element Content

Multi acid digest followed by solution analysis was used to determine the total available metal content of the core samples that could be potentially released to the environment. The results for the key parameters related to ARDML are summarised and compared to average crustal concentrations in Table 6.

Table 6. Whole Rock analysis, Hzradan waste rock.

Lithology	#	Al Aluminium	Sb Antimony	As Arsenic	Ba Barium	Cd Cadmium	Cr Chromium	Co Cobalt	Cu Copper	Fe Iron	Pb Lead	Mn Manganese	Mo Molybdenum	Ni Nickel	S Sulfur	Se Selenium	U Uranium	Zn Zinc
										mg/kg								
Average crustal abundance in mg/kg (Mason, 1966)		*81,300*	*0.2*	*1.8*	*425*	*0.2*	*100*	*25*	*55*	*50,000*	*13*	*950*	*1.5*	*75*	*260*	*0.05*	*1.8*	*70*
Chlorite Epidote Skarn—High Sulfur—Primary	2	5.0	1650.0	0.0	373	100.0	2370	100	1	89050	14	28	22.35	58	1	6.7	2.7	2
Chlorite Epidote Skarn—Low Sulfur—Primary	9	5.0	1411.1	0.0	444	100.0	1570	144	1	92256	12	27	19.78	44	0	5.5	5.3	1
Chlorite Epidote Skarn—Low Sulfur—Oxide	6	5.0	2200.0	0.0	592	100.0	2192	183	1	108800	11	33	16.03	31	0	7.1	5.8	2
Chlorite Skarn	2	5.0	22000.0	0.3	552	400.0	873	750	1	32700	19	28	23.50	75	0	6.1	7.2	1
Chert—High Sulfur—Primary	3	5.0	5633.3	0.3	557	866.7	1448	300	110	28833	16	30	22.47	81	0	12.1	4.0	1
Chert—Low Sulfur—Primary	11	5.0	8281.8	0.1	425	227.3	1353	291	8	42455	15	27	18.36	118	0	8.6	9.5	1
Chert—Low Sulfur—Oxide	4	5.0	3875.0	0.0	459	125.0	1430	225	1	52450	20	57	21.63	49	0	7.1	8.8	2
Garnet Skarn	3	5.0	200.0	0.0	451	100.0	1690	100	1	113500	12	23	23.20	78	0	10.1	20.1	2
Total/Average	40	5.0	5656.4	0.1	482	252.4	1616	262	16	70005	15	32	20.91	67	0	7.9	7.9	1

Arsenic, selenium and antimony were found to be elevated in all material types. Arsenic concentrations were approximately 3 to 12 times greater than average crustal abundance, with concentrations ranging between 10 & 17.2 mg/kg (average crustal abundance of 1.8 mg/kg). For antimony, enrichment varied from 3 times to greater than 12 times crustal abundance, with concentrations ranging between 0.6 & 2.5 mg/kg (compared to an average crustal abundance of 0.2 mg/kg). Selenium is generally enriched at greater than 12 times crustal abundance. There is also some elevated sulfur and manganese values within some of the material types. Sulfur is elevated within the high-sulfur chert and the chlorite skarn. The degree of enrichment in the chert high sulfur is the greatest of these with a concentration of 0.33% (compared with an average crustal abundance of 0.026%), and with enrichments of 0.17% in the chlorite skarn. These elevated sulfur concentrations will be related to the sulfide mineralisation within these material types, which at Hrazdan mainly consists of pyrite (FeS_2) with occasional chalcopyrite ($CuFeS_2$), pyrrhotite ($Fe_{1-x}S$), millerite (NiS), pentlandite (Fe,Ni)9S8 and galena (PbS). These three material types with an increased sulfur concentration are also associated with slightly elevated nickel, molybdenum and copper concentrations relative to the other material types. Although the presence of copper and nickel sulfide minerals only raise the whole rock concentrations to, at most, twice the average crustal abundance (Table 6), due to the nature of the reduced sulfide mineral, these elements are highly susceptible to mobilisation under oxidising conditions as demonstrated in the NAG test data later in this section.

The elevated manganese concentrations were restricted to the chlorite-epidote skarn material types, regardless of sulfur concentrations and degree of weathering. This elevation was typically around 3 to 4 times the average crustal abundance (~950 mg/kg) with a maximum enrichment of 3924 mg/kg.

3.6. Leach Tests

In particular the leaching of key parameters relating to ARDML was assessed to determine their potential mobility in the secondary environment. The leaching procedure utilised a single stage leach, with a liquid to solid ratio of 10 to 1. In general, leachates generated from the waste rock core materials were circum-neutral to moderately alkaline, with the chert lithologies generally more alkaline (pH ~9–9.5) than the chlorite epidote skarn lithologies (pH ~8.5–9 in Figure 9). The garnet skarn lithology had the lowest pH but was still circum-neutral whilst the chlorite skarn lithology had a leachate pH around 9.

There is a slight tendency for the samples containing the highest sulfur contents to release the greatest amounts of sulfate indicating that some dissolution of sulfide weathering products (i.e., potentially acid sulfate salts or non-acid sulfate salts such as gypsum) is taking place. However, any acid that may be liberated by dissolution of these minerals is being neutralised (Figure 10) by the excess of available acid buffering minerals.

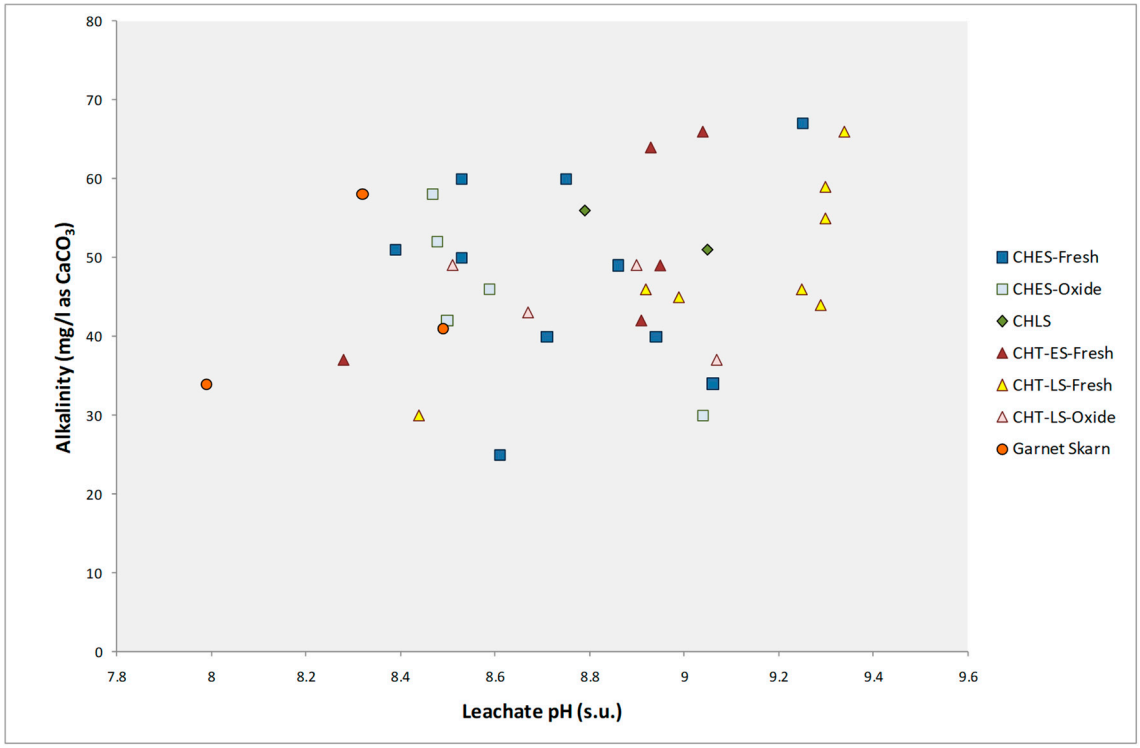

Figure 9. Relationship between leachate pH and alkalinity, deionized water leach.

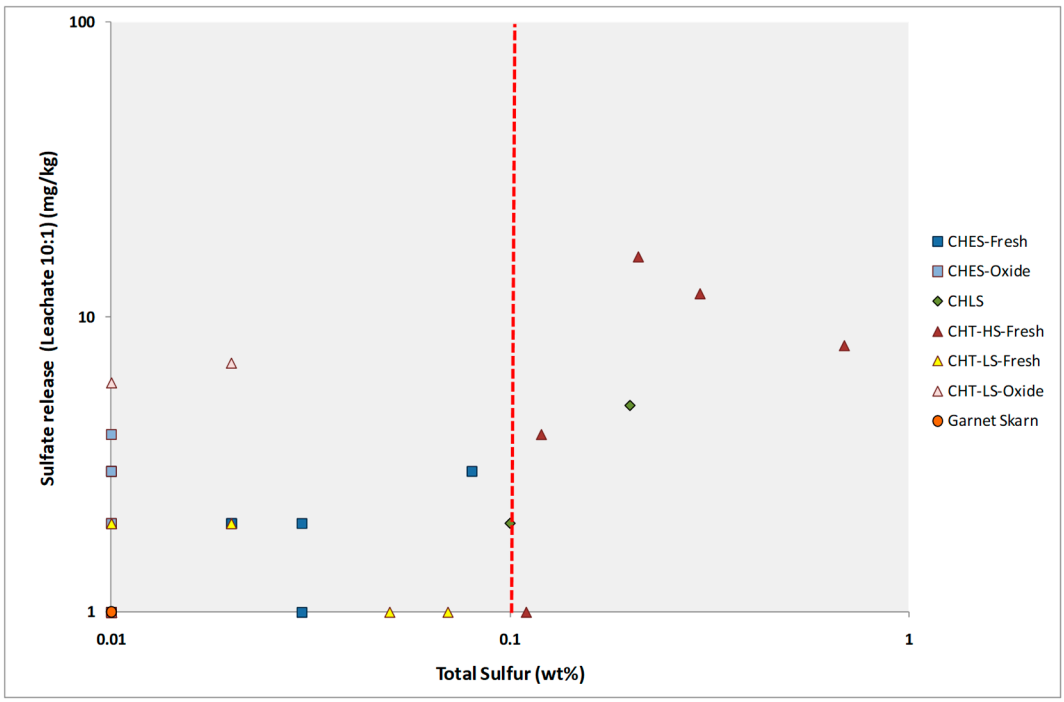

Figure 10. Scatter plot of Total sulfur vs. Sulfate sulfur release for the deionised water leach tests.

For arsenic and iron the results show they can be leached from one or more material types at relatively high concentrations with an apparent inverse relationship to each other but not to pH (Figure 11).

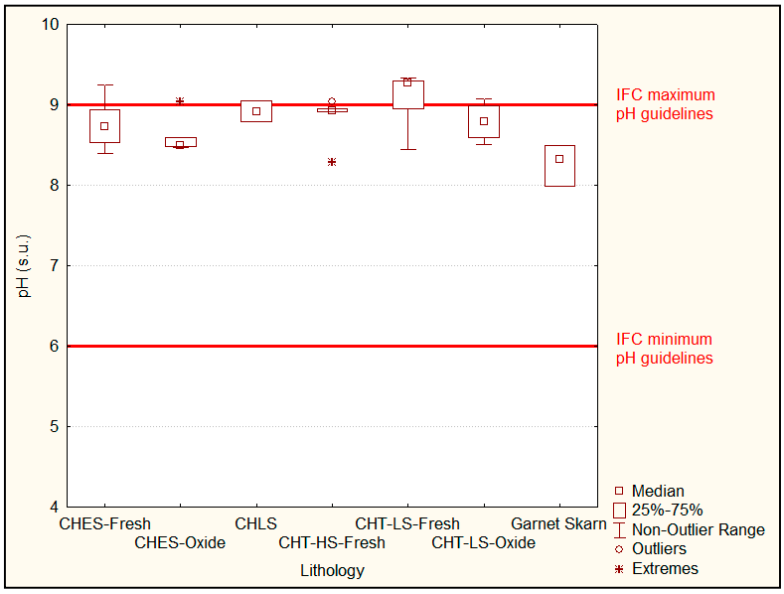
10
9
8
7
6
5
4
pH (s.u.)
IFC maximum
pH guidelines
IFC minimum
pH guidelines
CHES-Fresh
CHES-Oxide
CHLS
CHT-HS-Fresh
CHT-LS-Fresh
CHT-LS-Oxide
Garnet Skarn
Lithology
Median
25%-75%
Non-Outlier Range
Outliers
Extremes

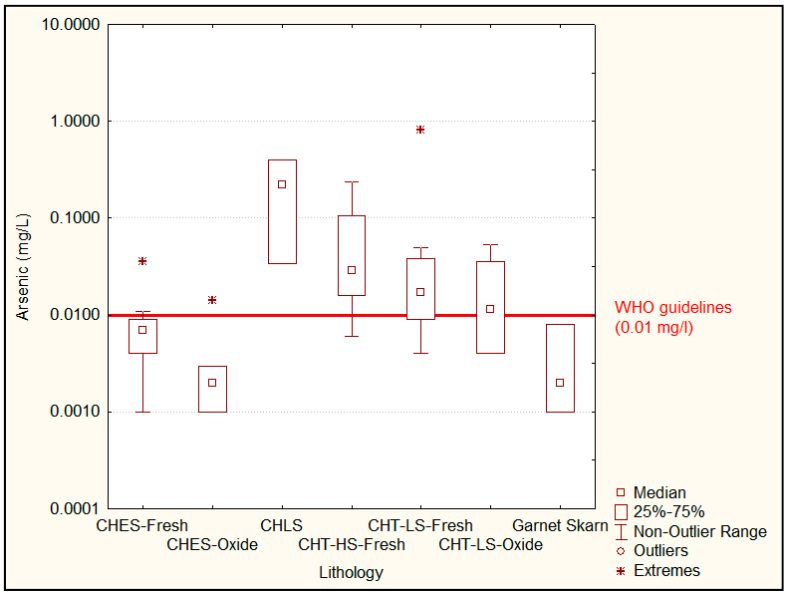
10.0000
1.0000
0.1000
0.0100
0.0010
0.0001
Arsenic (mg/L)
WHO guidelines
(0.01 mg/l)
CHES-Fresh
CHES-Oxide
CHLS
CHT-HS-Fresh
CHT-LS-Fresh
CHT-LS-Oxide
Garnet Skarn
Lithology
Median
25%-75%
Non-Outlier Range
Outliers
Extremes

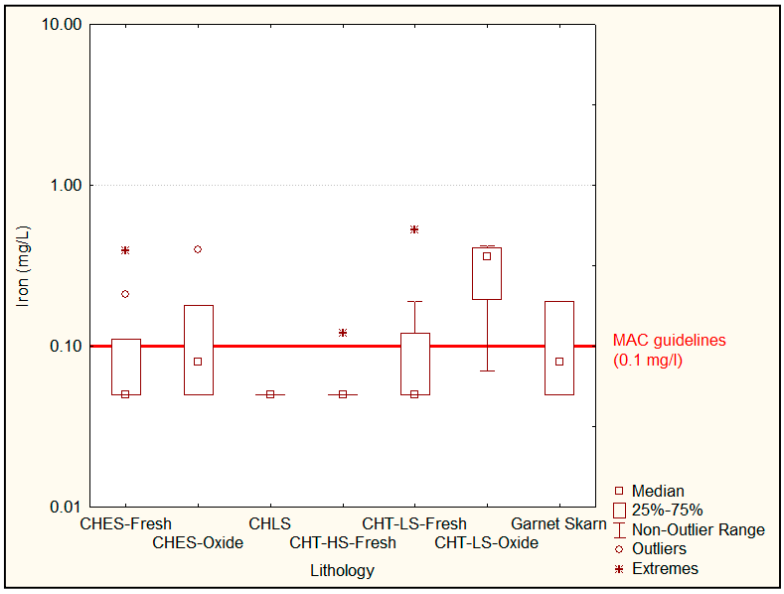

Figure 11. Box and whisker plots for pH, arsenic and iron release, deionized water leach.

The release of arsenic during the deionised leach at concentrations in excess of the World Health Organization guideline value of 0.01 mg/L indicates it is potentially the most problematic element at Hrazdan due to the human health risks it poses to people and the close proximity of a potable water supply (Figure 4) to the proposed mine site as well as to aquatic ecosystems. However, despite the elevated concentrations of arsenic in all material types (as identified in the multi element assay) it is only the chert and chlorite skarn material types that regularly exceed the guideline limits. A possible explanation for this is the presence of iron oxide and oxyhydroxide minerals (e.g., goethite [FeOOH]) in relatively high abundance within the chlorite-epidote skarn (CHES) and garnet skarns material types. At circum-neutral pH arsenic will strongly adsorb to iron oxyhydroxide minerals and therefore the presence of these minerals within these material types may be acting to attenuate the arsenic from the solution. This relationship is tentatively shown in Figure 12 which shows that those samples with the lowest total iron (as measured by the whole rock assay) show the greatest capacity to leach arsenic.

An aggressive hydrogen peroxide leach was undertaken on the waste rock core samples in order to assess the potential for high level metal release. This involved analysis of the NAG test leachate for a full suite of metal and metalloid ions. The results of the hydrogen peroxide leach for key parameters relating to ARDML are summarised in Table 7. This shows the amount of elemental leaching during the hydrogen peroxide leach compared to whole rock concentrations (as determined from the multi-element analysis) to allow determination of the potential mobility of enriched elements under intensive oxidising conditions

Table 7. Summary of hydrogen peroxide leach results for the waste rock samples. All values in mg/kg.

Lithology	Number	Al	Sb	As	Cd	Cr	Co	Cu	Fe	Pb	Mn	Mo	Ni	U	Zn
Chlorite Epidote Skarn—High Sulfur—Primary	2	4	0.10	0.1	0.01	3.50	0.10	0.10	5.0	0.10	0.30	0.25	0.50	0.10	0.70
Chlorite Epidote Skarn—Low Sulfur—Primary	9	31	0.12	0.2	0.01	1.92	0.10	0.11	5.0	0.10	0.22	1.46	0.10	0.10	0.54
Chlorite Epidote Skarn—Low Sulfur—Oxide	6	12	0.10	0.2	0.01	2.28	0.10	0.10	5.0	0.10	0.10	0.27	0.12	0.10	0.57
Chlorite Skarn	2	13	0.10	1.2	0.01	3.10	0.10	0.20	5.0	0.10	0.70	0.65	0.25	0.10	0.50
Chert—High Sulfur—Primary	3	43	0.10	0.8	0.07	2.70	10.8	9.67	5.0	0.10	22.13	1.63	73.43	0.10	15.67
Chert—Low Sulfur—Primary	11	15	0.16	0.6	0.01	3.00	0.96	0.24	5.0	0.10	4.03	2.75	5.68	0.10	0.82
Chert—Low Sulfur—Oxide	4	13	0.20	0.5	0.01	3.10	0.10	0.15	5.0	0.10	0.68	0.50	0.10	0.10	0.50
Garnet Skarn	3	31	0.13	0.5	0.01	2.77	0.10	0.33	5.0	0.10	0.17	0.13	0.10	0.10	0.60
Total/Average	40	20	0.1	0.5	0.0	2.8	1.5	1.4	5.0	0.1	3.5	1.0	10.0	0.1	2.5

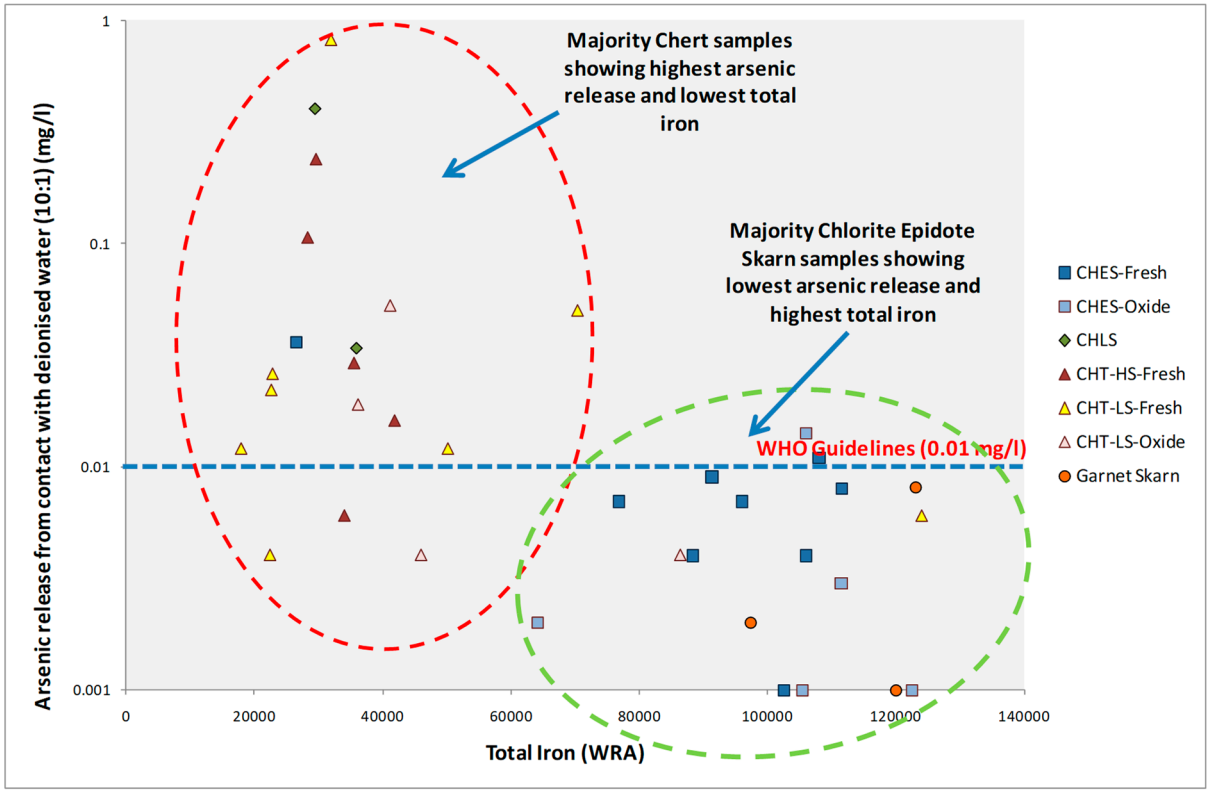

Figure 12. Plot of arsenic release from the deionised leach test against total iron from the whole rock assay.

Arsenic release is lower in the hydrogen peroxide leach than in the deionised water leach. This is thought to be due the artificially high redox conditions that develop in the hydrogen peroxide leach test resulting in all arsenic being oxidised to the As(V) form. The resulting oxyanion arsenate (AsO_4^{3-}) is strongly adsorbed to mineral surfaces at circum-neutral pH, especially iron oxides and therefore the resulting arsenic release is notably lower than would be expected under naturally occurring redox conditions [35].

3.7. Kinetic Tests

Static tests also show a potential for arsenic leaching due its relatively elevated concentrations observed during static testing and its high mobility even at neutral to alkaline pH. On that basis further work was undertaken to quantify that risk. The further testwork included humidity cell testwork to quantify the potential release rate of arsenic.

The full results of the humidity cell tests are presented in Supplementary Materials (Excel file "Hzradan"). With the exception of arsenic, all parameters have concentrations within the leachate that are below relevant guidelines. For arsenic, exceedances are observed, with only a slight decrease with time of the arsenic concentrations. The concentration of arsenic within leachate released from the humidity cells followed a similar pattern for all six humidity cells. This was an initial time lag of three week where the arsenic concentrations ramped up followed by a steady decline for the remaining 17 weeks. This steady decline can be explained by the observed enrichment within the pyrite rims which will give initially high values during sulfide oxidation followed by a generally steady decline. The results of the humidity cell tests for arsenic release over the first 20 weeks are summarised in Figure 13.

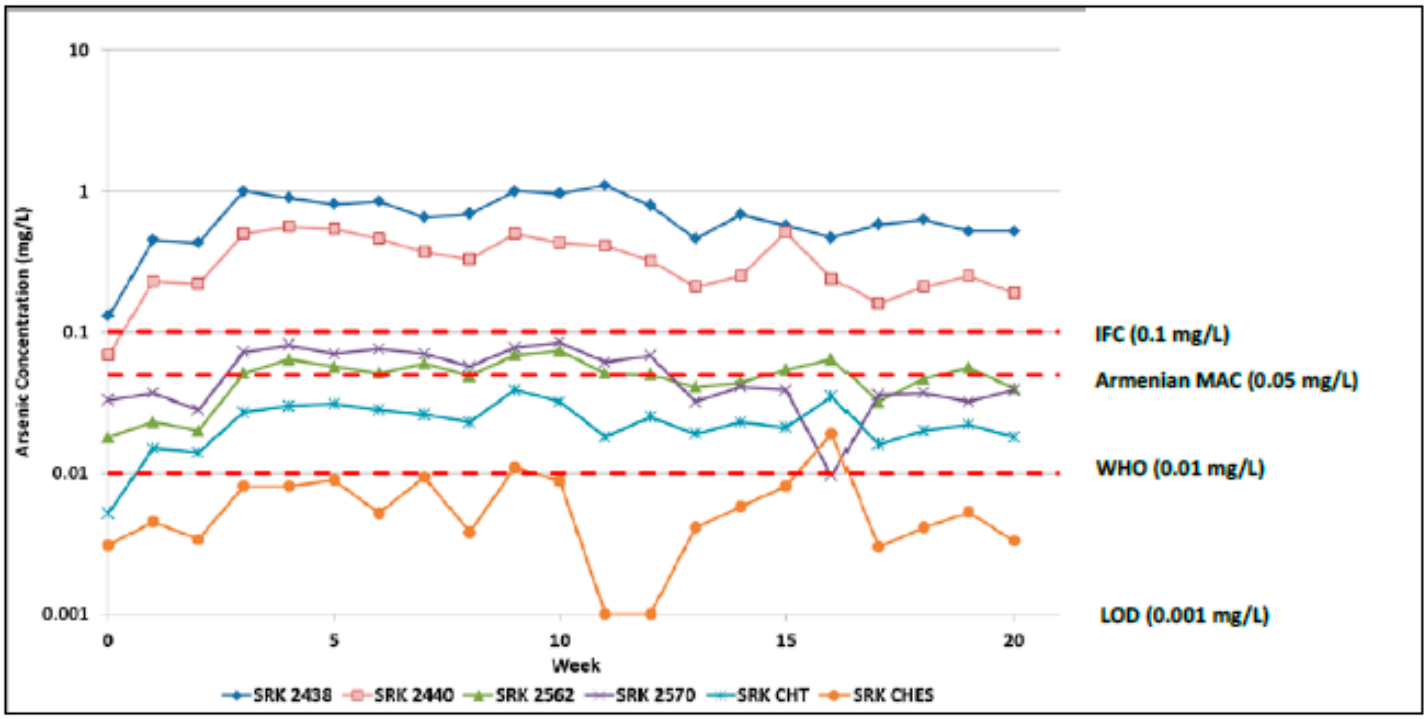

Figure 13. Time series plot of arsenic against weekly humidity cell cycle compared to IFC (top), WHO (middle) and Armenian MAC (bottom) guidelines, LOD (limit of detection).

Another interesting observation is that arsenic release is not dependent on arsenic 'head grade' but is related to sulfur content; cell SRK2438 shows the highest arsenic release concentrations despite containing one of the lowest arsenic head grades (Figure 13).

For all other elements analysed the concentrations observed within the leachate were below relevant IFC and WHO guidelines. On comparison with the Armenian water guidelines there are some elevated values for several parameters including Cr, Al, Cu, Mn, Ni, Se, V, Zn and Fe (see Supplementary Materials). For arsenic, exceedances are observed of all three guidelines, with only a slight decrease with time of the arsenic concentrations. The concentration of arsenic within leachate released from the humidity cells followed a similar pattern for all six humidity cells. This was an initial time lag of three weeks where the arsenic concentrations ramped up followed by a steady decline for the remaining 17 weeks.

4. Discussion

Based on the ARDML characterization undertaken in this study together with the associated background information including, but now limited to hydrogeology, geology, hydrology, climate, and engineering design, the following conceptual model and conceptual leaching conditions can be drawn. In addition, in the absence of suitable information on tailings ARDML it is assumed that the tailings material, ore and concentrate will behave in a similar manner to the most problematic waste rock samples. Based on the results of testing carried out in this report, there is potential for release of metals from the Hrazdan waste rock material.

The geochemical cycle of arsenic and other trace elements can be conceptualized for the Hzradan mine waste as shown in Figure 14. The placement of the waste rock material and the underlying strata being relatively permeable, it is likely that seepage from the WRD and tailings facilities will migrate vertically until they meet the water table. Potential contaminates contained within the seepage will then be transported along the groundwater flow path until such time as it is attenuated and or discharges to surface water (i.e., Hrazdan River, canal, wells or the local springs). In addition, surface run-off from mine waste facilities may also carry a contaminate load, especially prior to closure and re-

vegetation and therefore overland flow may also form a contaminate pathway. Metals likely to be released from the Hrazdan waste materials include arsenic, cobalt, copper, zinc, nickel, molybdenum, vanadium, manganese and nickel. Based on the source- pathway-receptor approach, there is potential for users of the surface water resources (including ecological users) to be negatively impacted and additionally there is potential for groundwater users to be impacted if appropriate mitigation measures are not taken into account.

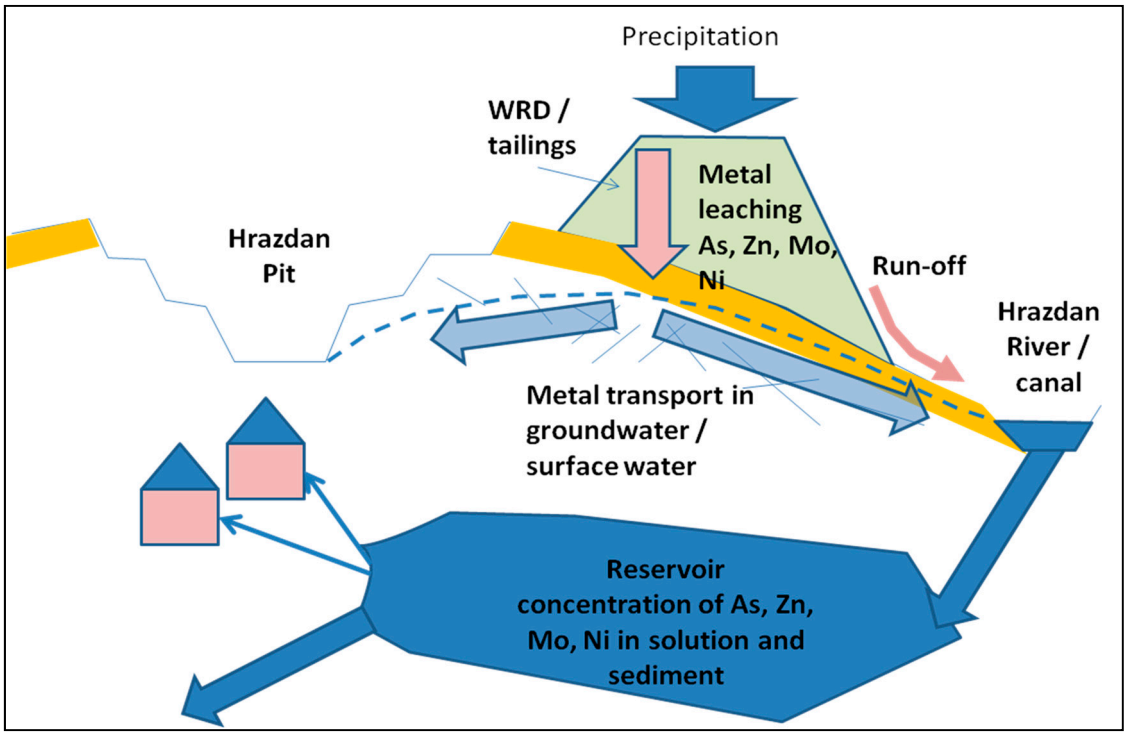

Figure 14. Geometallurgical model for arsenic leaching and acid generation within the Hrazdan waste rock**.** Red arrows indicate contaminated water from waste piles, blue comingled fresh and contaminated water as groundwater (light blue) or surface water (dark blue).

From the detailed mineralogical analysis to date it is apparent that the arsenic is primarily hosted by pyrite and iron-oxides and that the performance during humidity cell leaching is dependent on both the presence of pyrite which will release arsenic under natural weathering conditions and the presence of hydrous ferric oxide (HFO) sorption sites which will attenuate that release. Arsenic occur in solid solution or as nanoparticles in the pyrite [9]. Release of the element will be dependent on the oxidation of the pyrite versus formation of HFO phases and the rate of arsenate scavenging.

For samples 1 and 2 the comparatively high release of arsenic was not dependent on high whole rock assay concentrations (which were a fairly modest 14 and 46 mg/kg respectively) but on the lack of HFO which could not therefore attenuate that arsenic release. For samples 3 and 4 the arsenic concentrations were also fairly modest (20 and 21 mg/kg respectively) but the release rate was much lower. This is due to the slightly higher proportions of HFO within the sample which has partially attenuated that release. For the composite samples the arsenic release rate was lower still. This is likely to be a reflection of slightly higher proportions of HFO, and lower proportions of pyrite within the bulk of the waste rock.

The implications for this are that for sulfide-bearing waste rock (even at low concentrations of sulfide) there could be readily available arsenic for leaching throughout sulfide oxidation depending on the speciation of the As. As acid-generation is not a concern there are possible mitigation solutions that involve the blending or segregation of waste rock. In particular the iron-oxide bearing waste rock in this site showed much lower arsenic

release rates despite similar arsenic concentrations. It is therefore possible that suitably segregated, and used as a basal liner, that the iron-oxide bearing waste rock may have the residual capacity to attenuate any arsenic release from the waste rock as a whole. In order to test this, attenuation column tests and quantitative modelling of the results would be required, along with pilot scale field experiments to test proof-of-concept. Other trace elements such as Hg, Tl and Cd have constraints on their solubility in arsenian pyrite but this in itself could also be a factor in their release [11,15]. Oxidation of other sulfide minerals such as sphalerite are more likely to control their release [10].

In addition to these tests and taking account of the results it would be likely that further mitigation measures would be required. These would likely include the installation of lined perimeter drains to capture and treat toe seepage from the waste rock dump along with the possible installation of low-permeability cover. Given the sensitivity of ecological systems to arsenic contamination it would be necessary to install down-gradient monitoring wells to assess surface water and groundwater quality.

5. Conclusions

Contaminated-neutral drainage is generated at the Hrazdan project from depositing mine waste and its exposure to chemical weathering with metal(loids) released into waters courses at concentrations that exceed regulation criteria despite a lack of acid-generation. This was shown to be a potential problem during the Hrazdan Iron-Ore deposit where arsenic concentrations in humidity cell tests exceeded applicable water quality guidelines.

To better identify the source of arsenic and other trace elements in the mine waste the methodologies more commonly applied in Geometallurgy were adopted to identify the source of arsenic and likely mobilization pathways. The work has identified the importance of arsenic enriched rims in pyrite with an additional, less important host in hydrous ferric oxides (HFO). Whilst this HFO source may act as a potential attenuation mechanism for arsenic release the presence within pyritic rims is potentially problematic as future waste-rock dumps, if improperly designed, may release elevated levels of arsenic into local water courses through an initial concentrated release.

The use of detailed mineralogical studies using methods such as LA-ICP-MS and diagnostic leaching extractions pinpoint the source of the arsenic and these methods allow more precise interpretation of the environmental geochemistry testwork. It is therefore a general recommendation from this project that for feasibility level geochemical testing traditionally applied in mine waste projects would be improved by also applying typical geometallurgical methodologies in the characterization and assessment of mine waste.

Supplementary Materials: The following are available online at www.mdpi.com/article/10.3390/min11101085/s1: see Excel file "Hzradan".

Author Contributions: Conceptualization, R.B., C.B. and A.B., geological background A.V.; methodology R.B., C.B. and AB.; software, formal analysis C.B. and A.B..; writing—review and editing by R.B., C.B., A.B. and A.V. All authors have read and agreed to the published version of the manuscript.

Funding: Funding provided by Hrazdan mining company.

Data Availability Statement: Supplementary Materials file provides humidity cell data for samples

Acknowledgments: The authors would like to thank the Hrazdan mining company for approval to publish this study and colleagues at SRK for assistance on the project. We would also like to thank the reviewers who kindly reviewed this article.

Conflicts of Interest: The authors declare no conflict of interest.

References

1. Parbhakar-Fox, A.K.; Edraki, M.; Walters, S.; Bradshaw, D. Development of a textural index for the prediction of acid rock drainage. *Miner. Eng.* **2011**, *24*, 1277–1287
2. Brough, C.P.; Warrender, R.; Bowell, R.J.; Barnes, A.; Parbhakar-Fox, A. The process mineralogy of mine wastes. *Miner. Eng.* **2013**, *52*, 125–135
3. Lottermoser, B.G. *Mine Wastes. Characterisation, Treatment, Environmental Impacts*; Springer: Berlin/Heidelberg, Germany, 2010; p. 400
4. Nordstrom, D.K. Aqueous pyrite oxidation and the consequent formation of secondary iron minerals. *Acid Sulfate Weather.* **1982**, *10*, 37–56.
5. Nordstrom, D.K.; Alpers, C.N. Geochemistry of acid mine waters. In *The environmental geochemistry of mineral deposits, Part A: Processes, Techniques and Health Issues, Reviews in Economic Geology*; Plumlee, G.S., Logsdon, M.J., Eds.; Society of Economic Geologists: Denver, CO, USA: 1999; Volume 6A, pp. 133–160.
6. Jamieson, H.E. Geochemistry and mineralogy of solid mine waste: essential knowledge for predicting environmental impact. Elements **2011**, *7*, 381–386.
7. Jambor, J.L. Mineralogy of sulfide rich tailings and their oxidation products. In *The Environmental Geochemistry of Sulfide Mine Wastes*; Blowes, D.W., Jambor, J.L., Eds.; Mineralogical Association of Canada: Quebec, Canada, Short Course Series 22; 1994; pp. 59–102.
8. Ohlander, B.; Muller, B.; Axelsson, M.; ; Alakangas, L. An attempt to use LA-ICP-SMS to quantify enrichment of trace elements on pyrite surfaces in oxidizing mine tailings: *J. Geochem. Explor.* **2007**, *92*, 1–12
9. Deditius, A.P.; Utsunomiya, S.; Reich, M.; Kesler, S.; Ewing, R.C.; Houh, R.; Walshe, J. Trace metal nanoparticles in pyrite. *Ore Geol. Rev.* **2011**, *42*, 32–46.
10. Cook, N.; Ciobanu, C.L.; George, L.; Zhu, Z.Y.; Wade, B.; Ehrig, K. Trace element analysis of minerals in Magmatic-Hydrothermal ores by Laser Ablation Inductively Coupled Plasma Mass Spectrometry: Approaches and Opportunities. *Minerals* **2016**, *6*, 34.
11. Bowell, R.J.; Gingrich, M.; Bauman, M.; Tretbar, D.; Perkins, W.; Fisher, P. Occurrence of gold in the Getchell ores. *J. Geochem. Explor.* **1999**, *67*, 127–143.
12. Reich, M.; Simon, A.C.; Deditius, A.P.; Barra, F.; Chryssoulis, S.; Lagas, G.; Tardani, D.; Knipping, J.; Bilenker, L.; Sanchez-Alfaro, P.; et al. Trace element signature of pyrite from the Los Colorados Ion Oxide Apatite Deposit Chile: A missing link between Andean IOA and Ion Oxide Copper Gold systems. *Econ. Geol.* **2016**, *111*, 743–761.
13. MEND. *Review of Water Quality Issues in Neutral pH Drainage: Examples and Emerging Priorities for the Mining Industry in Canada*; Report 10.1; MEND: Ottawa, Canada, 2004.
14. Kwong, Y.T.J, *Thoughts on Ways to Improve Acid Drainage and Metal Leaching Prediction for Metal Mines*; US Geological Water Resources Investigations Report (USGS): Reston, VA, USA, 1995; pp. 95–4227.
15. Bowell, R.J.; Perkins, W.F.; Tahija, D.; Ackerman, J.; Mansanti, J. Application of LAICPMS to trouble shooting mineral processing problems at the Getchell mine, Nevada. *Miner. Eng.* **2005**, *18*, 754–761.
16. Plumlee, G.S. The environmental geology of mineral deposits. In *The Environmental Geochemistry of Mineral Deposits Part A: Processes, Techniques and Health Issues*; Plumlee, G.S., Logsdon, M.J., Eds.; Reviews in Economic Geology; Society of Economic Geologists: Littleton, CO, USA, 1999; Volume 6A, pp. 71–116.
17. Blanchard, M.; Alfredsson, M.; Brodholt, J.; Wright, K.; Catlow, C.R.A. Arsenic incorporation into FeS2 pyrite and its influence on dissolution: A DFT study. *Geochim. Cosmochim. Acta* **2007**, *71*, 624–630.
18. Berry, R.F.; Danyushevsky, L.V.; Goemann, K.; Parbhakar-Fox, A.; Rodemann, T. Micro-analytical technologies for mineral mapping and trace element deportment, In *Environmental Indicators in Metal Mining*; Lottermoser, B., Ed.; Springer International Publishing: Basel, Switzerland, 2016**;** pp. 55–72.
19. Fox, N.; Parbhakar-Fox, A.; Lottermoser, B. Prediction of metal mobility from sulfidic waste rocks using micro-analytical tools, Baal Gammon, Northern Australia. In *Environmental Indicators in Metal Mining*; Lottermoser, B., Ed.; Springer International Publishing: Basel, Switzerland, 2016; pp. 243–262.
20. Fox, N.; Parbhakar-Fox, A.; Lottermoser, B. Prediction of metal mobility from sulfidic waste rocks using micro-analytical tools, Spray, Tasmania. In *Environmental Indicators in Metal Mining*; Lottermoser, B., Ed.; Springer International Publishing: Basel, Switzerland, 2016; pp. 263–277.
21. Castellanos, E.S.; Maldonado, F. *Geologic map of the Republic of Armenia: U.S. Geological Survey Open-File Report 98-479, Map Scale 1:600,000*; USGS: Reston, VA, USA, 2000.
22. Bagdesaryan, G.P.; Gukasyan, R.K.; Karamyan, K.B. Absolute dating of Armenian ore formations. *Int. Geol. Rev.* **1969**, *11*, 1166–1172.
23. Adamia, S..A.; Chkoutua, T.; Kekelia, M.; Lordkipanidze, M.; Shavishvilli, I.; Zakraiadze, G. Tectonics of the Caucasus and adjoining regions: Implications for the evolution of the Tethys ocean. *J. Struct. Geol.* **1981**, *3*, 437–447.
24. Moritz, R.; Rezeau, H.; Pvtcharova, M.; Tayan, R.; Melkonyan, R.; Hovakimyan, S.; Ramazanov, V.; Selby, D.; Ulianov, A.; Chiaradia, M.; et al. Long-lived stationary magmatism and pulsed porphyry systems during Tethyan subduction to post-collision evolution in the southernmost Lesser Caucasus, Armenia and Nakhitchevan. *Gondwana Res.* **2016**, *37*, 465–503.
25. Hovakimyan, S.E.; Tayan, R.N. Fractures and mineralization controls. *Proc. Natl. Acad. Sci. Repub. Armen. Earth Sci.* **2008**, *61*, 3–12. (In Russian)

26. Gamkrelidze, I.P. Geodynamic evolution of the Caucasus and adjacent areas in Alpine times. *Bull. Georgian Acad. Sci.* **1997**, *155*, 391–394.
27. Adamia, S..A.; Zakriadze, G.; Chkhotua, T.; Sadradze, N.; Tsereteli, N.; Chabukiani, A.; Gventsdze, A. Geology of the Caucasus: A review. *Turk. J. Earth Sci.* **2011**, *20*, 489–544.
28. SRK. *Hrazdan Waste Rock Geochemical ARDML Characterisation Report*; 2012; SRK: Cardiff, UK; 65p.
29. GARD. Global Acid Rock Drainage Guide of The International Network for Acid Prevention (INAP). (GARD Guide). 2009. Available online: http://www.gardguide.com (accessed on: 09 March 2021).
30. Mason (1966) Principles of Geochemistry. John Wiley & Sons: London, UK. 3rd Edition, 329pp.
31. Standards Australia. *Wastes, Sediments and Contaminated Soils. Part 3: Preparation of Leachates—Bottle Leaching Procedure*; AS 4439.3-1997; 2019; Standards Autralia: Sydney, Australia.
32. ASTM. *Standard Test Method for Laboratory Weathering of Solid Material Using an Humidity Cell*; ASTM D 5744-13e1; ASTM International: Washington DC, USA, 2013.
33. Cornell RM, Schwertmann U. The Iron Oxides: Structure, Propertie, Reactions, Occurrences and Uses. Wiley-VCH, GmBH: Weinheim, Germany, 2003; Second Edition. 694p.
34. Evangelou, V.P.; Zhang, Y.L. A review: Pyrite oxidation mechanisms and acid mine drainage prevention. *Crit. Rev. Environ. Sci. Technol.* **1995**, *25*, 141–199.
35. Bowell, R.J. Arsenic sorption by Iron oxyhydroxides and oxides. *Appl. Geochem.* **1994**, *9*, 279–286.